Adsorbate-induced reconstruction by C 60 on close-packed metal surfaces Mechanism for different types of reconstruction

Shi, Xing-Qiang; Van Hove, Michel A.; Zhang, Rui-Qin

Published in:
Physical Review B - Condensed Matter and Materials Physics

Published: 21/02/2012

Document Version:
Final Published version, also known as Publisher's PDF, Publisher's Final version or Version of Record

Publication record in CityU Scholars:
Go to record

Published version (DOI):
10.1103/PhysRevB.85.075421

Publication details:
Shi, X-Q., Van Hove, M. A., & Zhang, R-Q. (2012). Adsorbate-induced reconstruction by C 60 on close-packed metal surfaces: Mechanism for different types of reconstruction. *Physical Review B - Condensed Matter and Materials Physics*, *85*(7), [75421]. https://doi.org/10.1103/PhysRevB.85.075421

Adsorbate-induced reconstruction by C_{60} on close-packed metal surfaces: Mechanism for different types of reconstruction

Xing-Qiang Shi, Michel A. Van Hove,* and Rui-Qin Zhang
Department of Physics and Materials Science, City University of Hong Kong, Hong Kong, China
(Received 16 January 2012; revised manuscript received 4 February 2012; published 21 February 2012)

Recent studies reveal that reconstruction of close-packed metal surfaces induced by C_{60} adsorption is the rule rather than the exception. Two types of reconstruction are reported for C_{60} on different surfaces: (1) C_{60} sinks into a 7-atom hole, such as on Cu(111); and (2) C_{60} sits over a 1-atom hole, such as on Ag(111) and Pt(111). An explanation for the preferred reconstruction type for different metals has been lacking. Here, we propose a criterion that predicts which reconstruction type should be expected: Namely, the formation of a 1- or 7-atom hole is determined only by the substrate geometric structure, including the surface lattice constant and the interlayer spacing; remarkably, the reconstruction type appears not to depend on the substrate electronic structure. Our intuitive geometrical explanation is validated by comparative first-principles calculations of the energetics of C_{60} on Cu(111), Ru(0001), Pt(111), and Ag(111) surfaces, listed here with increasing surface lattice constant. This provides a uniform explanation for the different reconstruction types that are observed experimentally for C_{60} on different close-packed metal surfaces. Moreover, our results provide a better explanation for the decomposition behavior of C_{60} on Ru(0001).

DOI: 10.1103/PhysRevB.85.075421 PACS number(s): 68.35.bp, 71.15.Nc, 68.43.−h

I. INTRODUCTION

The detailed bonding structure at the C_{60}-metal interface is of crucial importance for the electronic properties of adsorbed C_{60},[1,2] for its applications in molecular electronics,[3] and for its dynamic behavior on surfaces.[4] It is widely accepted that a strong interaction can induce the reconstruction of the substrate and/or a strain between the C_{60} molecules.[5–7] C_{60} adsorption on the highly symmetric close-packed fcc(111) and hcp(0001) metal surfaces has been the subject of many experimental and theoretical studies,[4,7–14] which demonstrate that the adsorption of C_{60} molecules often induces the reconstruction of close-packed metal surfaces.[9]

Two interface reconstruction types are observed for C_{60} on different close-packed metal surfaces, namely, formation of a 1- or a 7-missing-atom hole below each C_{60}, with C_{60} sitting over a 1-atom hole or sinking into a 7-atom hole, respectively.[7–12] However, many previous density functional theory (DFT) calculations only considered one of the two reconstruction types: e.g., only the 1-atom hole model was considered for C_{60} on Ag(111) and Ru(0001),[4,9] and only the 7-atom hole model was considered for C_{60} on Cu(111).[10] In previous DFT calculations, the two reconstruction types have been considered simultaneously only for C_{60} on two surfaces, Au(111) and Pt(111).[12,14] These studies show that the 7-atom hole structure is preferred for individual C_{60} molecules on Au(111),[14,15] while the 1-atom hole structure is preferred for a C_{60} monolayer on Pt(111).[12] However, for other close-packed metal surfaces, it has remained unclear which one of the two reconstruction types would actually be preferred. Therefore, in the current DFT study, we systematically compare both the 1- and the 7-atom hole models for C_{60} on several close-packed metal surfaces, including Cu(111), Ru(0001), Pt(111), and Ag(111), listed here with increasing surface lattice constant.

Our results show that for the metals with a smaller lattice constant, i.e., C_{60} on Cu(111) and Ru(0001), the 7-missing-atom hole model is favored, while for metals with a larger lattice constant, i.e., C_{60} on Pt(111) and Ag(111), the 1-missing-atom hole model is favored. These results for the preferred reconstruction type in the current study are consistent with the previous studies for C_{60} on Cu(111),[10] Pt(111),[7,8] and Ag(111),[9] while different from that reported for C_{60} on Ru(0001)[4] (however, the DFT calculations in that study neglected the 7-atom hole structure). Based on our comparative study of the reconstruction types on different metal surfaces with different lattice parameters, we propose that the reconstruction types only depend on the substrate geometric structure, which gives a unified explanation for the reconstruction types of C_{60} on different close-packed metal surfaces and agrees with all the existing experimental observations. Furthermore, the 7-atom hole structure on Ru(0001) can better explain the decomposition behavior of C_{60} on Ru(0001).[4]

II. COMPUTATIONAL METHOD

The DFT calculation details are the same as in our previous study.[12] We adopt the Vienna Ab initio Simulation Package (VASP)[16–18] in the local-spin-density approximation,[19,20] which has been shown to be able to describe both the energetic and electronic properties of C_{60} on metal surfaces.[4,9,12–14,21–23] The Projector Augmented Wave (PAW) potentials are used to describe the core electrons.[24–26] The cutoff energy is 400 eV for the plane-wave basis set describing the valence electrons. A seven-layer slab is used to simulate the metal surfaces. The unit cell sizes and shapes are well defined experimentally for the ordered phases of C_{60} on Cu(111), Pt(111), and Ag(111),[7–10] corresponding to about one monolayer (ML, defined here as the saturation coverage of the first adsorbed layer); for C_{60} on Ru(0001), the adsorption was studied at less than 1 ML in a recent scanning tunneling microscopy (STM) study[4] and is therefore less ordered. In accord with the experimental observations for C_{60} on Cu(111), Pt(111), and Ag(111), we study the following unit cells in this work: Cu(111)-(4×4)-C_{60}, Pt(111)-$(\sqrt{13} \times \sqrt{13})$R13.9°-

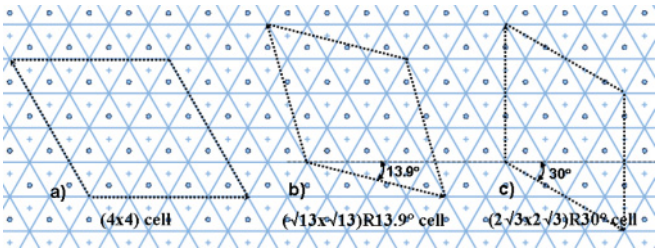

FIG. 1. (Color online) Sketch of three supercells defined on fcc(111) metal surfaces. Blue solid lines denote the ideal top metal layer lattice, while circles and crosses denote the deeper layers.

C_{60}, Pt(111)-$(2\sqrt{3} \times 2\sqrt{3})$R30°-$C_{60}$, and Ag(111)-$(2\sqrt{3} \times 2\sqrt{3})$R30°-$C_{60}$, respectively. Note that for C_{60} on Pt(111), two ordered phases are observed, and the two phases can be experimentally isolated through careful tuning of the preparation conditions.[12] There are three supercells containing 16, 13, and 12 metal surface atoms per unit cell, respectively, before reconstruction. These three supercells, defined on a closed-packed metal surface, are sketched in Fig. 1, using an fcc(111) surface as an example. For C_{60} on Ru(0001), since the unit cell is not yet well defined experimentally,[4] we consider both adsorption at 1 ML and at less than 1 ML. Specifically, we consider two configurations, Ru(0001)-$(\sqrt{13} \times \sqrt{13})$R13.9°-$C_{60}$ and Ru(0001)-(4×4)-C_{60}, corresponding to about 1 ML and about 13/16 ML, respectively.

For the binding geometries in the reconstructed adsorption, we assume adsorption with a C_{60} hexagonal ring down, parallel to the metal surface, which is determined from previous STM, low-energy electron diffraction (LEED), surface x-ray-diffraction (SXRD), and DFT studies.[4,7–12] We also consider different binding geometries with C_{60} rotated around the surface normal. For the 7-atom hole adsorption structures, C_{60} sinks into the *top* metal layer and sits above a hollow site of the *second* metal layer (see Fig. 2). In this case, C_{60} as well as the *top-layer* metal atoms are all placed either above fcc hollow sites or above hcp hollow sites of the *second* metal layer (in the latter case forming a dislocation within the metal). Our results favor C_{60} as well as the *top-layer* metal atoms placed above the fcc hollow site of the *second layer* for the fcc metals, and above the hcp hollow site for the hcp metals, thus continuing the bulk lattice type into both the reconstructed layer and the C_{60} overlayer. In addition to the 1- and 7-atom hole models, we also considered 3- and 6-atom hole models, which we find to be less favored than either the 1-atom or the 7-atom hole model.[14] In the following discussions, we focus on the most stable geometries (see supplementary material.[27])

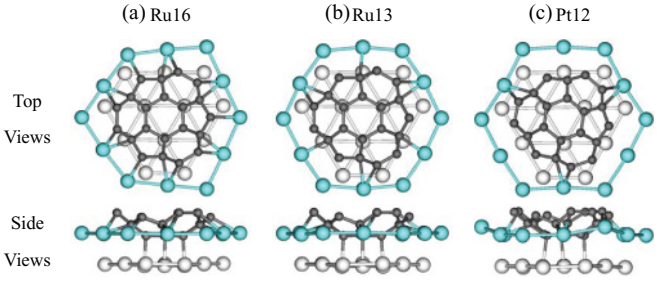

FIG. 2. (Color online) Local adsorption geometries for the three kinds of 7-atom hole configurations with three kinds of unit cells, using (a) Ru16, (b) Ru13, and (c) Pt12 (see text) as examples. To better show the local adsorption structures, only the bottom part of C_{60} is included (dark gray circles and bonds); to better compare the local structures with different cells, all nearby metal atoms surrounding a C_{60} molecule are shown, which include atoms beyond one unit cell. Some of these (light blue/medium gray circles and bonds) form the edge of the 7-atom hole in the outermost metal layer. Black/blue (medium gray) bars show C-metal bonds smaller than 2.28 Å. Second-layer metal atoms (light gray circles and bonds) are also shown.

III. RESULTS AND DISCUSSIONS

For the (clean, unreconstructed) closed-packed metal surfaces, the experimental surface lattice constant, from small to large, is 2.56 Å for Cu(111), 2.71 Å for Ru(0001), 2.77 Å for Pt(111), and 2.89 Å for Ag(111). The nearest molecular center-to-center distance for C_{60} in its three-dimensional (3D) bulk fcc phase is about 10.0 Å. In order to match the projected area of one C_{60} molecule, about 16 surface atoms in Cu(111) are needed, or about 13 surface atoms in Pt(111) and Ru(0001), or about 12 surface atoms in Ag(111). Therefore, different unit cells (Fig. 1) are needed for different metal surfaces to contain one C_{60} molecule, which is consistent with the corresponding experimental observations.[4,7–12] For convenience in the following, we will call the different structures "Cu16" for Cu(111)-(4×4)-C_{60}, "Ru16" for Ru(0001)-(4×4)-C_{60}, "Ru13" for Ru(0001)-$(\sqrt{13} \times \sqrt{13})$R13.9°-$C_{60}$, "Pt13" for Pt(111)-$(\sqrt{13} \times \sqrt{13})$R13.9°-$C_{60}$, "Pt12" for Pt(111)-$(2\sqrt{3} \times 2\sqrt{3})$R30°-$C_{60}$, and "Ag12" for Ag(111)-$(2\sqrt{3} \times 2\sqrt{3})$R30°-$C_{60}$ (since $4 \times 4 = 16$, $\sqrt{13} \times \sqrt{13} = 13$, and $2\sqrt{3} \times 2\sqrt{3} = 12$)). Basically, we are comparing C_{60} on four metal surfaces with different surface lattice constants. For each of the three unit cells, we consider two metals: Cu16, Ru16; Ru13, Pt13; Pt12, Ag12, and for each of these six configurations, we compare the 1- and 7-atom hole geometries, resulting in 12 geometries altogether, for which the energetics are listed in Table I.

TABLE I. Adsorption energies (in eV) corrected for vacancy formation energies ($E_{ads} + E_{vac}$) for various 1- and 7-atom hole structures, listed by increasing bulk metal lattice constant from Cu to Ag. Bold values show the favored hole type for each structure, while underlined values emphasize the difference in the favored hole type between Ru and Pt. The numbers without and with parentheses are calculated using a different approach in accounting for the vacancy formation energies: migration of "missing" hole atoms to bulk vs kinked-edge sites, respectively (see further below).

($E_{ads} + E_{vac}$)	1-atom hole	7-atom hole
Cu16	−2.36 (−2.70)	**−3.93** (−5.27)
Ru16	−5.06 (−5.08)	**−7.20** (−7.77)
Ru13	−5.01 (−5.03)	**−6.71** (−7.28)
Pt13	**−5.22** (−5.34)	−5.01 (−5.32)
Pt12	**−4.79** (−4.91)	−3.76 (−4.07)
Ag12	**−2.17** (−2.18)	−1.24 (−1.45)

A. Mechanism of reconstructions with 7- or 1-atom holes

Figure 2 shows three kinds of 7-atom hole geometries, i.e., local C_{60}-metal binding geometries for three kinds of unit cells with 16, 13, and 12 metal surface atoms per unreconstructed layer, using Ru16, Ru13, and Pt12 as examples, respectively. With the 7-atom hole adsorption, C_{60} sinks into the 7-atom hole and sits above the hollow site of the second layer (on the fcc hollow site for fcc metals and on the hcp hollow site for hcp Ru). For the geometries with different cells, there are always three metal atoms of the second metal layer binding with C_{60} (see Fig. 2), while the number of metal atoms in the top layer binding with C_{60} varies with different unit cells and increases with the number of metal atoms per unit cell in the top surface layer.

After the 7-atom hole formation, the number of remaining surface metal atoms per unit cell is $16 - 7 = 9$, $13 - 7 = 6$, and $12 - 7 = 5$ for Ru16, Ru13, and Pt12, respectively. Note, however, that in order to better exhibit the local adsorption geometries, Fig. 2 shows all metal atoms surrounding one C_{60} molecule, which include metal atoms beyond one unit cell. For the (4×4) cell with a 7-atom hole, all of the nine remaining metal atoms bind with C_{60}, which makes the 7-atom hole geometry favorable (see Table I for the energies of Cu16 and Ru16). For the $\sqrt{13}$ cell with a 7-atom hole, fewer (six vs nine) atoms are left per unit cell in the top layer, but they also all bind with C_{60}; in this case, the 7-atom hole geometry is relatively less strongly favored than the 1-atom hole geometry (see Table I for the energies of Ru13 and Pt13; the delicate underlying mechanism will be elaborated in the following subsection). For the $2\sqrt{3}$ cell, only five metal atoms are left per unit cell in the top layer, and only three of them bind with C_{60} due to the mismatch of symmetry between the C_{60} and the five atoms,[28] which makes the 7-atom hole geometry unfavorable (see Table I for the energies of Pt12 and Ag12). We conclude, for the 7-atom hole geometries with different cells (from $[4 \times 4]$ to $\sqrt{13}$ to $\sqrt{12}$), that the number of top-layer metal atoms that bind to C_{60} changes considerably (from nine to six to three atoms), and the preference of the reconstruction types changes from the 7-atom hole geometry to the 1-atom hole geometry with increasing lattice constant (or with decreasing number of atoms per layer inside one unit cell). In other words, as the metal lattice constant increases, the 7-atom hole leaves a relatively smaller number of metal atoms to participate in the metal-C bonding, weakening the relative overall adsorption energy per molecule.

For the 1-atom hole geometries, Fig. 3 shows that the local C_{60}-metal binding is largely independent of unit cell: There are always six metal atoms that bind with C_{60}. From this independence of unit cell, we conclude that the preference of the 7- or 1-atom hole geometries for different metals indeed is mainly due to the change in the number of atoms binding with C_{60} in the 7-atom hole geometries. Note that formation of a 7-atom hole requires a considerably larger vacancy formation energy than formation of a 1-atom hole, as will be discussed in more detail later herein. As a result, to make the 7-atom hole geometry become favorable, it must have more metal atoms binding with C_{60} than does the 1-atom hole geometry. So the final result is a competition between the gain of adsorption energy E_{ads} and the cost of vacancy formation energy E_{vac},

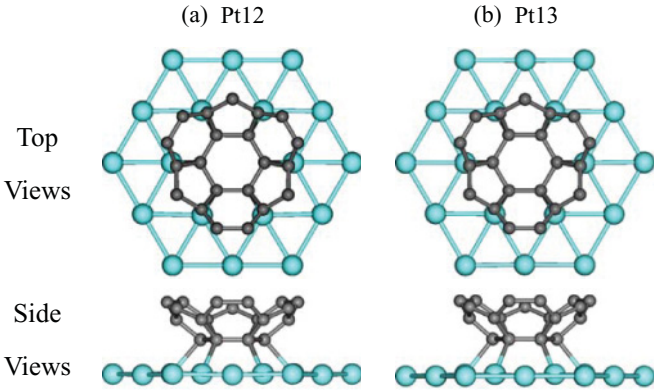

FIG. 3. (Color online) Local adsorption geometries for the 1-atom hole structures with different unit cells, using Pt12 and Pt13 (see text) as examples. For the surface layer, atoms beyond one unit cell are shown. Color codes: C (dark gray), Pt (light blue/medium gray).

so the final result is determined by $(E_{ads} + E_{vac})$, as will be discussed in the following subsection.

B. Energetics

To compare the energetics of the adsorption geometries with 1- and 7-missing-atom holes (these geometries have different numbers of atoms), we calculate the adsorption energies E_{ads} corrected for vacancy formation energies E_{vac}, i.e., $(E_{ads} + E_{vac})$ as listed in Table I. The adsorption energy is calculated as $E_{ads} = E_{C60+Surf} - (E_{Surf} + E_{C60})$, where $E_{C60+Surf}$ is the energy of the combined C_{60}/metal system, E_{Surf} is the energy of the bare surface with a 1- or 7-missing-atom hole (optimized independently), and E_{C60} is the energy of a C_{60} molecule in the gas phase. Our method of calculating the vacancy formation energies E_{vac} will be discussed in Subsection C.

Table I lists the adsorption energies corrected by vacancy formation energies for various 1- and 7-atom hole structures. As the bulk metal lattice constant increases (from Cu to Ag), the surface unit cell size changes from (4×4) to $(2\sqrt{3} \times 2\sqrt{3})$, in order to give C_{60} the constant space it needs. For the smallest bulk lattice constant (Cu16), the 7-atom hole structure is clearly favored, while for the largest bulk lattice constant (Ag12), it is the 1-atom hole structure that is clearly favored. From the previous discussion for Fig. 2, we already know the reason for this: The difference in the surface lattice constant results in different unit cells and different numbers of metal atoms binding with C_{60}. However, for the intermediate lattice constant values (Ru and Pt), either the 7-atom hole (for Ru) or the 1-atom hole (for Pt) may be preferred, and this preference depends on further structural details: Besides the lattice constant, we must also consider the interlayer spacings of the two metals. Comparing the ideal (unreconstructed and unrelaxed) surfaces, the interlayer spacings are 2.26 Å for Pt(111) and 2.14 Å for Ru(0001), so the interlayer spacing for Ru is smaller by about 0.12 Å than for Pt. For the 7-atom hole geometry, this smaller interlayer spacing in Ru allows C_{60} to bind more strongly with the second layer than for Pt (as can be seen by comparing the C-metal bond lengths with the sum of the covalent radius of C and metal atoms, cf. Table II): This is the reason why C_{60} on Ru(0001) prefers a 7-atom hole, while

TABLE II. C-metal bond lengths (in Å) of C_{60} with the second metal layer in the (assumed) 7-atom hole structures of Pt and Ru, which is compared with the sum of the covalent radii of C (in sp^3 configuration) and the respective metal atoms.

	C-metal bond lengths	Sum of covalent radii
C_{60}/Ru(0001)	2.08	2.22
C_{60}/Pt(111)	2.11	2.12

on Pt(111) it prefers a 1-atom hole. The smaller interlayer distance of Ru compared to Pt comes from the following two factors: (1) hcp Ru has a lattice-constant ratio c/a of 1.58, which is smaller than the ideal c/a ratio of about 1.63; and (2) Ru has a slightly smaller surface lattice constant than Pt.

C. Vacancy formation energies

To properly calculate and compare the vacancy formation energies for the 1- and 7-missing-atom hole structures in the top layer (upon which C_{60} molecules are adsorbed), one must decide where to place the missing atom(s): One may choose to add these metal atom(s) into the bulk phase (without disturbing the bulk structure, as is often done without good justification) or in the gas phase (as unbonded gas atoms, which is not realistic); both options provide possible energy references.[4] However, these are extreme options (with 12 or 0 nearest neighbors for the missing atom) that can easily over- or underestimate the vacancy energies. A more realistic scenario follows the more probable fate of the missing atoms in the experiment, namely, incorporation at a kinked-edge site along a terrace, which is normally present on real surfaces. This provides an intermediate binding configuration for the missing

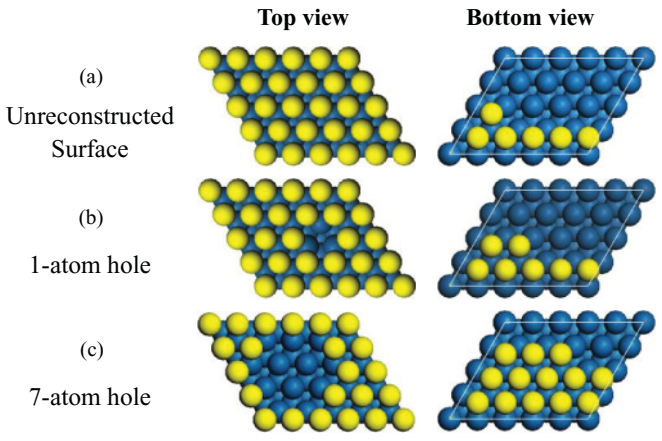

FIG. 4. (Color online) Structural slab models used to calculate the vacancy formation energies, showing one two-dimensional (2D) unit cell (outlined) and both top views (middle column) and bottom views (right column). Yellow (light gray) balls denote the atoms in the top and bottom layers. (a) Unreconstructed top layer, with a kinked-edge site at the bottom layer; (b) 1-missing-atom hole at the top layer, and one added atom at a kinked-edge site in the bottom layer; (c) 7-missing-atom hole in the top layer, and seven added atoms at successive kinked-edge sites in the bottom layer. These plots use the fcc(111) surface as an example; the same idea of kinked-edge models can also be directly applied to the hcp(0001) surface.

TABLE III. Vacancy formation energies E_{vac} (in eV) calculated for missing atoms placed in kinked-edge sites (Fig. 4; numbers without parentheses) and for missing atoms placed in bulk sites (numbers in parentheses).

E_{vac}	1-atom hole	7-atom hole
Cu(111)	+1.08 (+0.74)	+3.23 (+1.89)
Ru(0001)	+1.86 (+1.84)	+6.07 (+5.50)
Pt(111)	+1.61 (+1.49)	+4.55 (+4.24)
Ag(111)	+0.89 (+0.88)	+2.74 (+2.53)

atom, with typically six nearest neighbors (a kinked-edge site is more likely than a straight-edge site, which provides typically five nearest neighbors). So, the most logical way to deal with the surface missing atoms should be to place them at kinked surface step edges. For our calculations of the vacancy formation energies, we thus constructed kinked-edge models as shown in Fig. 4. Starting with an unreconstructed top layer [Fig. 4(a), left panel], we construct a kinked-edge site at the bottom layer [Fig. 4(a), right panel], which will later "receive" a missing atom from the top layer. Next, we can move one or seven atoms out of the top layer, making a 1- or 7-atom hole, and put them at kinked-edge sites in the bottom layer [see Fig. 4(b) and 4(c)]. The vacancy formation energy for the 1-atom hole is then calculated from the energy difference between the structures of Fig. 4(b) and 4(a) (without C_{60}). Similarly, the vacancy formation energy for the 7-atom hole is calculated from the energy difference between the structures of Fig. 4(c) and 4(a). The three models in Fig. 4 all have the same number of atoms (also when the molecule is included on the top layer), making it possible to directly compare their total energies.

Finally, we point out that, for comparison, we also calculated the total energies by placing missing atoms in bulk sites: We then obtained the same preference for the 1- or 7-atom hole adsorption geometry of C_{60}, although the energy values are clearly different (cf. Table III). Although the most common approach leads to the same structural preference in this particular case, this will not always be true in general (especially when comparing smaller energy differences).

D. Further discussion of the mechanism of reconstruction types

We have shown here, by comparing the preferred reconstruction types of C_{60} on different metal surfaces, that the reconstruction type depends primarily on geometric aspects of the substrate, including mainly the surface lattice constant and also the interlayer spacing (the latter for the comparison between Pt and Ru, with similar surface lattice constant but different relative interlayer spacings). In the following, we further point out that the preference for a reconstruction type does not depend on the electronic structure of the substrate.

We make the following *a priori* surprising observations. The reconstruction type is the same (a 1-atom hole) for C_{60} on the electronically dissimilar metals Ag and Pt; it is also the same (but now a 7-atom hole) for C_{60} on the electronically dissimilar metals Cu and Ru. By contrast, different reconstruction types are found for Ag vs Cu, even though both Ag and Cu have full *d* bands; also, different

reconstruction types are found for Pt vs Ru, while the *d* bands of neither Pt nor Ru are full; compared to Ag and Cu, Pt and Ru have *d* bands much closer to the Fermi level.[29–32] As a result, we must conclude that the reconstruction types do not depend on the substrate electronic structure; we think this is due to the fact that the interface reconstruction is thermally activated by higher annealing and deposition temperatures, which can substantially change the structural and hence also the electronic properties of the substrate (high temperatures can induce substantial changes of the surface structures, such as adatoms, holes, and long-range reconstructions; these local and global changes in the surface structure result in electronic structure changes locally or even globally), while the lattice spacing (supercell size) remains largely unchanged.

A larger substrate lattice constant results in a smaller number of metal atoms per C_{60} area (and thus per supercell). Hence, a smaller hole will be formed, because the remaining number of surface atoms binding with C_{60} cannot become too small: At least six atoms in the top layer binding to C_{60} are needed [as shown in Fig. 2(b)] for the 7-atom hole geometry to be favored. This also explains why for C_{60} on Pt(111) the relative instability of the 7-atom hole structure compared to the 1-atom hole structure is larger for Pt12 (with three of the five remaining atoms per cell binding to C_{60}) than for Pt13 (with six atoms binding to C_{60}). In Table I, the energy difference between the 1- and 7-atom hole structures becomes larger for Pt12 compared to Pt13. Note that due to the 3-fold rotational symmetry of C_{60} and the metal surfaces, the number of metal atoms in the top layer binding to C_{60} can be nine, six, or three, but cannot be five.

To better understand how the number of remaining surface metal atoms per cell determines the type of reconstruction induced by C_{60}, it is useful to count C-metal bonds within different supercells. For this purpose, it is convenient to focus on the 7-atom hole edge composed of 12 metal atoms forming a hexagonal ring (distorted hexagonal ring after relaxation, see the 12 top-layer metal atoms in Fig. 2): This hexagonal ring is present in the (4×4), $(\sqrt{13} \times \sqrt{13})$R13.9°, and $(2\sqrt{3} \times 2\sqrt{3})$R30° supercells, which are predetermined by the metal lattice constant. The crucial difference between supercells lies in the degree to which the ring edge and its atoms are shared between neighboring holes: More sharing weakens C-metal bonds and makes the 7-atom hole less favorable. In the (4×4) cell [Fig. 2(a)], the hexagonal edges share six corner atoms, while the six other edge atoms are not shared and are closer to the location of the C_{60}. The latter atoms thus form six strong unshared C-metal bonds, while the former atoms split into two groups after structural relaxation. Focusing on one unit cell, three of them bond with one C_{60} in this unit cell, while the other three bond with C_{60} in adjacent unit cells. In the $(\sqrt{13} \times \sqrt{13})$R13.9° cell [Fig. 2(b)], neighboring holes share more of their edges, such that each metal atom bonds closely to one C_{60} in one hole and simultaneously more weakly to a more distant C_{60} in an adjacent hole, weakening all C-metal bonds (after relaxation, these 12 metal atoms also split into two groups: Again focusing on one unit cell, six of them bond with C_{60} in this unit cell, while the other six bond with C_{60} in adjacent unit cells). Finally, in the $(2\sqrt{3} \times 2\sqrt{3})$R30° cell [Fig. 2(c)], the edges of adjacent holes are completely shared, so that six of the metal edge atoms each make two C-metal bonds (to two molecules), thereby weakening both, while the six other corner metal atoms are each shared by three molecules (without chemical bond formation); here also, after relaxation, the six metal edge atoms split into two groups: three of them bond with C_{60} in the one unit cell, while the other three bond with C_{60} in adjacent unit cells. (A counterargument in the foregoing reasoning is that with shrinking unit cell, each remaining surface metal atom loses more metal neighbors, so that the remaining metal-metal bonds could become stronger with shrinking unit cell, thus favoring the 7-atom hole; however, the C-metal bonds are stronger than metal-metal bonds, and this tips the balance in favor of more C-metal bonds and against more metal-metal bonds.)

E. C_{60} decomposition on Ru(0001)

Decomposition of C_{60} on Ru(0001) has been observed via STM studies.[4] It was demonstrated that C_{60} is a unique precursor compared to C_2H_4 for the formation of geometrically well-defined graphene quantum dots on a Ru(0001) substrate. The authors also observed the embedding of C_{60} molecules in the Ru(0001) surface before decomposition.[4] Here, we try to give some insight into the decomposition of C_{60} through the obtained 7-atom hole structure. We will analyze this issue from three aspects: (1) the C_{60}-Ru bond numbers; (2) the C-C bond elongation due to C-Ru bonding; and (3) the C_{60}-Ru binding strength (binding energy) relative to other C_{60}-metal binding.

(1) Analysis from C_{60}-Ru bond numbers: (a) The 7-atom hole geometry is more favorable than the 1-atom hole geometry for decomposing C_{60} since more C-Ru bonds are formed in the 7-atom hole geometry; and (b) C_{60} adsorption at less than 1 ML favors cage-opening more than at 1 ML, because more metal atoms bind with C_{60} at less than 1 ML [compare Fig. 2(a) and 2(b), and the energies in Table I for Ru16 and Ru13], which agrees with the STM experiment reporting cage-opening at less than 1 ML conditions.[4]

(2) Analysis from the C-C bond elongation: We consider the C-C bond elongations at the bottom of C_{60}, including the bottom hexagon and the surrounding hexagons and pentagons, which partly bind with the metal surface atoms, as shown in Fig. 5(a). The C-C bonds shown in yellow in Fig. 5(b) are elongated and thus weakened the most, by ∼5% relative to

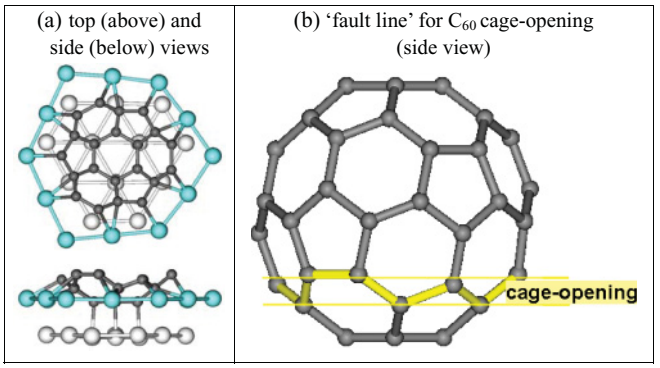

FIG. 5. (Color online) (a) Assumed local adsorption geometry of Ru(0001)-(4×4)-C_{60} with a 7-atom hole; and (b) the "fault line" (yellow/light gray lines and bonds) for cage-opening of C_{60} on Ru(0001) (the Ru surface at bottom is not shown).

free C_{60}; the C-C bonds below and above the "yellow bonds" are elongated much less, by less than 3% for the bonds below and by less than 2% for the bonds above. So, the weakened C-C bonds shown in yellow in Fig. 5(b) define a possible "fault line" for cage-opening of C_{60} on Ru(0001). The largest bond elongation reported in Ref. 4 with a 1-atom hole model is 3%, which is smaller than the 5% elongation found in our 7-atom hole model. The larger bond elongation seen in our 7-atom hole model thus favors C_{60} decomposition on Ru(0001).[4]

(3) Analysis from the binding energy: Comparing the energies listed in Table I, C_{60} binds more strongly to Ru than to other metals—This is another argument for the possibility of cage-opening of C_{60} on Ru.

IV. CONCLUDING REMARKS

We have discussed the reconstruction types of C_{60} on Cu(111), Ru(0001), Pt(111), and Ag(111) through a comparative DFT study. Based on these four surfaces, a mechanism is proposed for their reconstruction types: The geometric structural details of the substrate determine the formation of 1- or 7-atom holes, rather than their electronic structures. Also, our 7-atom hole model can better explain the decomposition behavior of C_{60} observed on Ru(0001), by the weakening of C-C bonds by relatively strong Ru-C bonds.

We are aware of an apparent exception to our criterion in the case of C_{60} on Au(111). Although the lattice constant of Au is close to Ag, it is found that for the individually adsorbed C_{60} molecules on the so-called "elbow sites," the adsorption configuration can be the 7-atom hole structure.[14] However, the situation is substantially different from that considered here in several ways: Clean Au(111) already has a "herringbone reconstruction," where the "elbow site" is more reactive because it already has one missing Au atom,[33] unlike clean nonreconstructed Cu, Pt, Ag, or Ru. Also, the coverage of C_{60} on Au(111) is much lower than 1 ML. In addition, a very recent STM study demonstrates that for a C_{60} *monolayer* on *nonreconstructed* Au(111), the adsorption contains a mixture of molecules, some of which induce 1-atom hole reconstruction (with a hexagon down), while others induce nonreconstructed adsorption (with a "C-C 6:6 bond" down).[34]

We are also aware that C_{60} adsorption on Al(111) may have a more complicated (6×6) reconstruction.[13] However, the (6×6) reconstruction is believed to be very close to the 1-atom hole model but not close to the 7-atom hole model. The lattice constant of Al is close to Ag (Ag prefers a 1-atom hole). So, our mechanism still works for Al(111). For C_{60} on Ni(111), with a lattice constant close to that of Cu, a surface reconstruction behavior very similar to that of C_{60} on Cu(111) has been observed in a STM experiment,[35] and this also further strengthens support for our proposed mechanism.

ACKNOWLEDGMENTS

This work was supported in part by the Hong Kong Research Grant Council GRF Grant CityU 102707, and the High Performance Cluster Computing Centre, Hong Kong Baptist University, which receives funding from the Research Grants Council, University Grants Committee of the Hong Kong Special Administrative Region, and Hong Kong Baptist University.

*vanhove@cityu.edu.hk

[1] Y. Yamada, S. Yamada, T. Nakayama, M. Sasaki, and T. Tsuru, Jpn. J. Appl. Phys. **50**, 08LB06 (2011).
[2] L. Wang, W. Chen, and A. T. S. Wee, Surf. Sci. Rep. **63**, 465 (2008).
[3] G. Schull, T. Frederiksen, A. Arnau, D. Sánchez-Portal, and R. Berndt, Nature Nanotech. **6**, 23 (2011).
[4] J. Lu, P. S. E. Yeo, C. K. Gan, P. Wu, and K. P. Loh, Nature Nanotech. **6**, 247 (2011).
[5] W. W. Pai and C.-L. Hsu, Phys. Rev. B **68**, 121403(R) (2003).
[6] C.-L. Hsu and W. W. Pai, Phys. Rev. B **68**, 245414 (2003).
[7] C. D. Liu, Z. H. Qin, J. Chen, Q. M. Guo, Y. H. Yu, and G. Y. Cao, J. Chem. Phys. **134**, 044707 (2011).
[8] R. Felici, M. Pedio, F. Borgatti, S. Iannotta, M. Capozi, G. Ciullo, and A. Stierle, Nat. Mater. **4**, 688 (2005).
[9] H. I. Li, K. Pussi, K. J. Hanna, L.-L. Wang, D. D. Johnson, H.-P. Cheng, H. Shin, S. Curtarolo, W. Moritz, J. A. Smerdon, R. McGrath, and R. D. Diehl, Phys. Rev. Lett. **103**, 056101 (2009).
[10] W. W. Pai, H. T. Jeng, C. M. Cheng, C. H. Lin, X. D. Xiao, A. D. Zhao, X. Q. Zhang, G. Xu, X. Q. Shi, M. A. Van Hove, C. S. Hsue, and K. D. Tsuei, Phys. Rev. Lett. **104**, 036103 (2010).
[11] G. Xu, X. Q. Shi, R. Q. Zhang, W. W. Pai, and M. A. Van Hove, unpublished (2012).
[12] X. Q. Shi, A. B. Pang, K. L. Man, R. Q. Zhang, C. Minot, M. S. Altman, and M. A. Van Hove, Phys. Rev. B **84**, 235406 (2011).
[13] M. Stengel, A. De Vita, and A. Baldereschi, Phys. Rev. Lett. **91**, 166101 (2003).
[14] L. Tang, X. Zhang, Q. M. Guo, Y. N. Wu, L.-L. Wang, and H.-P. Cheng, Phys. Rev. B **82**, 125414 (2010).
[15] Note that the experiment of Ref. 14 focused on the individually adsorbed C_{60} molecules on the "elbow sites" of the Au(111) surface "herringbone reconstruction," for which the coverage is much smaller than one monolayer.
[16] G. Kresse and J. Furthmüller, Phys. Rev. B **54**, 11169 (1996).
[17] G. Kresse and J. Furthmüller, Comput. Mater. Sci. **6**, 15 (1996).
[18] G. Kresse and J. Hafner, Phys. Rev. B **47**, 558 (1993).
[19] D. M. Ceperley and B. J. Alder, Phys. Rev. Lett. **45**, 566 (1980).
[20] J. P. Perdew and A. Zunger, Phys. Rev. B **23**, 5048 (1981).
[21] W. L. Yang, V. Brouet, X. J. Zhou, H. J. Choi, S. G. Louie, M. L. Cohen, S. A. Kellar, P. V. Bogdanov, A. Lanzara, A. Goldoni, F. Parmigiani, Z. Hussain, and Z. X. Shen, Science **300**, 303 (2003).
[22] V. Brouet, W. L. Yang, X. J. Zhou, H. J. Choi, S. G. Louie, M. L. Cohen, A. Goldoni, F. Parmigiani, Z. Hussain, and Z. X. Shen, Phys. Rev. Lett. **93**, 197601 (2004).
[23] L.-L. Wang and H.-P. Cheng, Phys. Rev. B **69**, 165417 (2004).
[24] P. E. Blöchl, Phys. Rev. B **50**, 17953 (1994).

[25]G. Kresse and D. Joubert, Phys. Rev. B **59**, 1758 (1999).
[26]P. E. Blöchl, C. J. Först, and J. Schimpl, Bull. Mater. Sci. **26**, 33 (2003).
[27]See Supplemental Material at http://link.aps.org/supplemental/10.1103/PhysRevB.85.075421 for relaxed atomic coordinates.
[28]Note that there is a slight but distinct rotation of C_{60} around the surface normal in Pt12 [see Fig. 2(c) for the three twisted C-metal bonds between the bottom C_{60} hexagon and the second-layer metal atoms], which is due to the binding of C_{60} with the top-layer 3 metal atoms.
[29]N. V. Smith, Phys. Rev. B **9**, 1365 (1974).
[30]J. E. Rowe and N. V. Smith, Phys. Rev. B **10**, 3207 (1974).
[31]A. Ruban, B. Hammer, P. Stoltze, H. L. Skriver, and J. K. Nørskov, J. Mol. Catal. A: Chem. **115**, 421 (1997).
[32]Also see the projected density of states (PDOS) plots in the following web site: [http://www.icmm.csic.es/jcerda/EHT_TB/TB/Periodic_Table.html].
[33]P. Maksymovych, D. C. Sorescu, D. Dougherty, and J. T. Yates, J. Phys. Chem. B **109**, 22463 (2005).
[34]L. Tang, Y. Xie, and Q. Guo, J. Chem. Phys. **135**, 114702 (2011).
[35]C. H. Lin, K. C. Lin, T. B. Tang, and W. W. Pai, J. Nanosci. Nanotechnol. **8**, 602 (2008).